

# Anticipation and next action forecasting in video: an end-to-end model with memory

Fiora Pirri, Lorenzo Mauro, Edoardo Alati, Valsamis Ntouskos, Mahdieh Izadpanahkakhk, Elham Omrani  
ALCOR Lab, Sapienza University of Rome, Italy

{pirri,mauro,alati,ntouskos,izadpanahkakhk,omrani}@diag.uniroma1.it

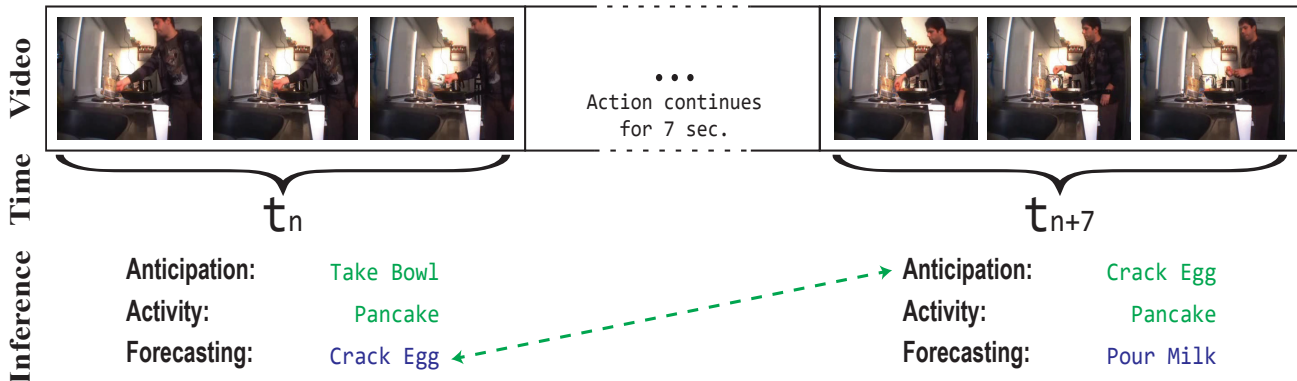


Figure 1: Anticipation and next action forecasting with no time limits.

## Abstract

Action anticipation and forecasting in videos do not require a hat-trick, as far as there are signs in the context to foresee how actions are going to be deployed. Capturing these signs is hard because the context includes the past. We propose an end-to-end network for action anticipation and forecasting with memory, to both anticipate the current action and foresee the next one. Experiments on action sequence datasets show excellent results indicating that training on histories with a dynamic memory can significantly improve forecasting performance.

## 1 Introduction

There is nowadays an extraordinary amount of contributions to the challenging task of future events prediction, from a single image, a short video clip or a video. A number of these contributions focus on anticipating actions recognition as earliest as possible [8, 19, 26, 33] obtaining significant results in reducing anticipation time. Others predict the features of a frame about seconds in the future [23, 8, 42, 7]. Other contributions focus on predicting motion trajectories, considering trajectory-based human activity [14], dense trajectories [44] or subsequent human movement paths [42], which is quite relevant in team activities, especially sports.

Recently, [6] have extended long-term anticipation up to 5 minutes, assigning action labels to each frame in the temporal horizon of anticipation.

A common denominator of the mentioned contributions is the analysis of actions beyond the visible frames, taking into account different scene features. Some have highlighted the relevance of objects for affordance [19], others the scene context, others the human motion or the analysis of past events. Proposed methods range from encoder-decoder models [7] to generative models [24], to variational autoencoders [44], and inverse reinforcement learning [46].

Here we introduce a new variant of these ideas conjugating anticipation of the current action with forecasting the next unseen one. Given few frames of a human activity video, we can both anticipate the current action label and foresee the next one, independently of how long the current action will last. The idea is shown in Figure 1.

This variant of anticipation, requiring to foresee a completely unseen action, is useful in several contexts. It is quite relevant to infer goals and intentions. In team sports, like soccer, it is useful for pursuing a specific game schema. In robotics it is useful for helping someone in accomplishing a task: knowing that after the current action a specific action might occur it would be possible for a robot to collect tools or predispose some machinery to provide help.

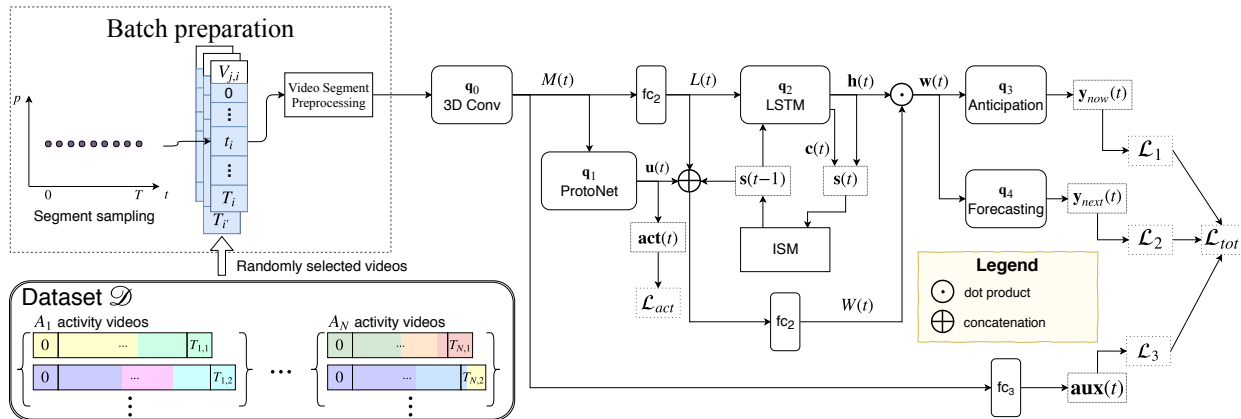


Figure 2: Schema of the Anticipation and Forecasting Network.

## 2 Overview and Contribution

The main novelty of this work is the combination of anticipation of current action with forecasting the next unseen action by learning from the past, using an accumulating memory. Forecasting a next unseen action is challenging and it requires to anticipate to an early stage the recognition of the current action. Further, it requires to discriminate plausible future actions filtering out those that are implausible. Finally, it requires to understand the context of the current action, and a relevant part of the context is the past, for mastering action evolution.

To solve these problems we introduce a new end-to-end Anticipation and Forecasting Network (AFN) with memory to dynamically learn from past observations. The network schema is illustrated in Figure 2. AFN anticipates the recognition in an untrimmed video from 6 frames scattered in one second, examining several scenes and body elements, including motion and body pose for the current action and the action history. We fix the anticipation to one second to cope with the starting time uncertainty. Further, a relevant component of AFN, besides the memory, is a ProtoNet [38] predicting which activity an action belongs to. Finally, based on the current action anticipation, AFN forecasts the next action, independently of the time horizon.

We illustrate our results on different baselines, considering all the newly introduced aspects. In particular, the anticipation is confronted with other methods on two datasets used by several approaches, namely JHMDB [11] and UCF101 [39]. Forecasting is shown on four datasets Breakfast[20], Charades [35], CAD120 [18] and MPII cooking dataset [30]. We show that for both anticipation and forecasting, AFN outperforms the state of the art on these datasets. In the lack of a specific metric, we have introduced appropriate measures, detailed in Section 5.

## 3 Related Work

Since the early work of [14] and [31] a wealth of works focused on anticipation, prediction, and forecasting human actions, because is such a challenging and attractive research problem. So far the terms anticipation, prediction and forecasting have been used as fungible terms to estimate what shall occur in frames, which are not yet observed. There is a difference, though. A first distinction is between the pixel level approaches on the human motion [23], path trajectories [10, 2, 45] and image generation [43] and the approaches focusing on anticipating (predicting, forecasting) action labels. A general overview is given in [42] and [15]. A further difference is between anticipation and forecasting. Here we exemplify the distinction as follows. While anticipation requires a percentage of the current action to be observed, forecasting presumes that no frames of the foreseen action are observed. For this reason a number of datasets have recently been proposed with long-term activity videos lasting minutes, where actors perform sequences of complex actions [20, 5, 34, 35].

**Action anticipation** Action anticipation has been widely considered in the literature. Here we focus only on recent results on anticipation of action labels, more details can be found in [42] and [15]. Recently, [29] introduced tailored loss functions by applying dynamic images to a generative model for actions anticipation. They benchmark their results mainly on JHMDB [11], UT-Interaction [32] and UCF101 [39]. Singh *et Al.* [37] jointly evaluate online spatio-temporal action localization and prediction via a single shot multi-box detector. Similarly, as [29]. They benchmark on UCF101 (though considering 24 actions) and JHMDB datasets. The deep action tube network extended in [36] has been designed in order to predict past, present, and future focusing on 10% of the video. It has been evaluated on JHMDB dataset. Kong *et Al.* [16] propose a combined

CNN and LSTM along with a memory module in order to record “hard-to-predict” samples, they benchmark their results on UCF101 and on Sports-1M [12] datasets. In [33] an RNN with an RBF kernel is proposed to improve the performance of feature mapping for the anticipation task. Their benchmarks are on JHMDB, UCF101 with 24 actions, and UT interaction. Lai *et Al.* [22] optimize a global-local based temporal distance model and a two-stream network model. They benchmark their work on UCF11, the UCF YouTube Action Dataset [25] and on the HMDB with 51 actions. The work of [1] develops a multi-stage LSTM network integrating both the context and action aware representations. They evaluated their work on the UCF101, UT-Interaction, and JHMDB datasets. Considering the history trend, [7] applies a reinforced encoder-decoder to anticipate the next representation of an action. They evaluate their work on UCF101 and on TVSeries datasets.

Except [36] and [7], none of the above methods seems to focus on the past to anticipate actions. In fact, one of the contribution of our model is the addition of a memory component, which can deal with long sequences so as to learn from the action history both anticipation and forecasting. Also we confront with a larger set of actions from UCF101, JHMDB and other also for forecasting, reporting results significantly better than the cited ones, because the model proposed can learn from scattered sequences.

**Forecasting future actions** Forecasting unseen frames has been early introduced in [23] and [43], the latter one promoting a significant amount of research on generating future frames based on generative adversarial networks. On the other hand, forecasting labels for unseen actions frames has not yet been widely developed, due to the fact that it is an ill-posed problem. As far as we know only [4, 27] and [6] have faced forecasting for action labels. While [27] use ground truth (in particular on MPII cooking activities dataset [30] and VIRAT dataset [28]) to forecast next action, we do not. Moreover, we can do both anticipation and forecasting on untrimmed video. Similarly to our work Farha *et Al.* [6] have recently tackled the anticipation challenges by inferring current and future actions via an RNN-HMM for anticipation and CNN for predicting the time horizon and the activity label. Like them, we use Breakfast [20] for forecasting and Charades [35] as a second dataset, in place of 50Salads [40]. The advantage of our approach is that we can combine anticipation and forecasting. Furthermore, as shown in the results section, we can foresee next action independently of time limits, and with greater accuracy.

## 4 Anticipation and Forecasting Network

The Action Forecasting Network (AFN) is the proposed end-to-end network. AFN aims at both anticipating the current action and forecasting the next action. To obtain the desired results we resort to several components. To analyze the immediate previous frames we add deep convolutional layers of a C3D network. To establish the activity the action belongs to (in case activities are subdivided into actions) we add a ProtoNet. To take into account the history of the previous actions we add an RNN network with *lstm* cells and an internal dynamic memory. Finally, we use several fully connected layers to connect the components and to both classify the current action and forecast the next one. As explained in §4.2, a relevant novelty of AFN is the ability to elaborate arbitrary long action sequences thanks to the introduction of an internal state memory collecting the internal states of the RNN network components. A visual representation of the network is illustrated in Figure 2.

### 4.1 Input

For the video datasets of activities taken into account, activities often allocate sequences of different actions, see Section 5 for details. Therefore, given all the videos and activities taken from a chosen dataset, the input batch for a single run of the AFN network collects videos both considering a number of activities and of actions. More specifically, we consider a dataset as

$$\mathcal{D} = \{A_j = (a_{j,1}, \dots, a_{j,m}) | j=1, \dots, N \text{ and } m > 0\} \quad (1)$$

Where  $A_j$  is an activity from a set of  $N$  activities in the dataset  $\mathcal{D}$  and the  $a_{j,k}$  are the actions the activity  $A_j$  might be decomposed into. For each activity  $A_j$  there is a varying number of videos available. The input batch to AFN is formed as follow. First we sample randomly from all the videos of all the activities in  $\mathcal{D}$  a fixed number  $\xi$  of videos, resulting in a sample of  $K$ ,  $K < \xi$  of different activities. Further, we sample a segment of 6 RGB frames scattered on a time lapse of one second for each video. From the sampled RGB frames we compute two heat maps of the human pose (see [3]): one for the human joints and the other for the human limbs. We compute also the optical flow for each frame. This information is stacked as four more channels in addition to the RGB ones. Finally, all six frames, for each video, are collected into a single tensor as follows:

$$X_{j,i}(t_i) = \pi(V_{j,i}(t_i)), \quad t_i \sim \text{Unif}(0, T_i), \quad i=1, \dots, \xi \\ T_i = \text{length}(V_{j,i}) \text{ in seconds}, \quad j = 1, \dots, K \quad (2)$$

Here  $\pi$  is the above described sampling and preprocessing of the 6 frames sample,  $V_{j,i}$  denotes the  $i$ -th video of  $A_j$ ,

$j = 1, \dots, K$ , and  $t_i$  is the time index, randomly sampled from a uniform distribution in the interval  $[0, T_i]$ , with  $T_i$  the length of the video  $V_{j,i}$ , in seconds. Therefore, an input batch is formed by the tensors  $X_{j,i}$ . In the following when we focus on a single tensor, we drop the indexes both from  $X$  and from  $t$ .

## 4.2 Internal State Memory

To allow AFN to take into account the history of the whole previous sequence we introduce an Internal State Memory (ISM), which stores the internal states of the RNN network with *lstm* cells [9] (indicated, resp., as ISM and  $q_2$  in Figure 2). In this way every computation takes as input a single sample and the internal state corresponding to the previous second. For every video in the dataset, a state vector  $\mathbf{v} \in \mathcal{S}^{T \times 512} \subseteq \mathbb{R}^{T \times 512}$  is defined as:

$$\mathbf{v} = \begin{pmatrix} \mathbf{s}(0) \\ \vdots \\ \mathbf{s}(T) \end{pmatrix} \quad (3)$$

Here  $\mathbf{s}(t) = (\mathbf{h}(t)^\top, \mathbf{c}(t)^\top)^\top$ ,  $t \in [0, T]$ , are the  $q_2$  states. Given  $t$  we define  $\mathbf{s}(t-1)$  as:

$$\mathbf{s}(t-1) = \begin{cases} \mathbf{0} & \text{if } J(t) = 0 \\ \mathbf{s}(t-1)^{J(t)} & \text{otherwise} \end{cases} \quad (4)$$

Here  $J(t)$  denotes the number of times that  $t$  was sampled up to the current training step.

Given the preprocessed input  $X(t)$  and the internal state  $\mathbf{s}(t-1)$  the  $q_2$  component produces, beside the outputs, a new internal state  $\mathbf{s}(t)^{J(t)}$ . This new state is then used to update the states vector  $\mathbf{v}$  (see eq. 3).

The collection of all the state vectors forms the ISM. Note that at inference time, samples are taken sequentially.

## 4.3 Anticipation and next action prediction

The first component of AFN are the 5 convolutional layers of C3D [41], denoted  $q_0$ , in Figure 2. This  $q_0$  component computes a feature tensor taking  $X(t)$  (see eq. 2) as input:

$$M(t) = q_0(X(t)). \quad (5)$$

The tensor computed by  $q_0$  has size  $(7 \times 7 \times 512)$  and is further reduced in size by a fully connected network  $f_{c_k}$ , where  $k$  indicates the network layers, here  $k = 2$ .

$$L(t) = f_{c_k}(M(t)) \quad (6)$$

The next component is  $q_2$ , introduced in §4.2, which computes the vector:

$$\mathbf{s}(t) = (\mathbf{h}(t)^\top, \mathbf{c}(t)^\top)^\top = q_2(L(t), \mathbf{s}(t-1)) \quad (7)$$

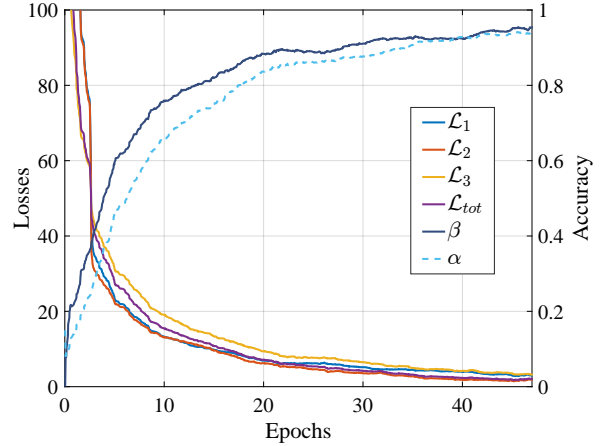


Figure 3: Training loss and accuracy per epochs.

Here  $\mathbf{s}(t)$  and  $\mathbf{s}(t-1)$  are  $q_2$  states and the way they are selected from the ISM is described in the previous paragraph 4.2.

At this point we introduce an advisory component  $q_1$  supplying  $q_2$  output with further information. This information is collected by a fully connected network, which learns the weights used to dynamically influence  $\mathbf{h}(t)$ . More precisely, these weights are defined as follows:

$$W(t) = \text{vec}^{-1}(f_{c_k}([L(t), \mathbf{s}(t-1), \mathbf{u}(t)])) \quad (8)$$

Here  $L(t), \mathbf{s}(t-1), \mathbf{u}(t)$  are concatenated,  $f_{c_k}$  is a fully connected layer with  $k = 1$ ,  $L(t)$  is the tensor obtained in eq. 6 and  $\mathbf{u}(t)$  is the latent vector obtained by the component  $q_1$ . The component  $q_1$  is a prototypical network, detailed in §4.4, which predicts the activity the current input belongs to, hence it provides relevant information, restricting the search space for the final classification. The notation  $\text{vec}^{-1}$  used in eq. 8 indicates the inverse of the vectorization operator, namely  $\text{vec}^{-1} : \mathbb{R}^{nm} \rightarrow \mathbb{R}^{m \times n}$ .

The weight matrix  $W$  of size  $256 \times 256$  is finally multiplied by the  $q_2$  output ( $t$ ), obtaining the vector  $\mathbf{w}(t)$ :

$$\mathbf{w}(t) = W(t)\mathbf{h}(t) \quad (9)$$

The last classification component is  $q_3$ , anticipating the current action as follows:

$$\mathbf{y}_{now}(t) = q_3(\mathbf{w}(t)) = \sigma(f_{c_k}(\max(0, \mathbf{w}(t) + \mathbf{b}_{now}))) \quad (10)$$

where  $\sigma(x_j) = e^{x_j} / \sum_{j=0}^K e^{x_j}$  is the softmax,  $\mathbf{b}_{now}$  is the bias, and  $K$  are the action classes.

Finally,  $\mathbf{y}_{now}(t)$  and  $\mathbf{w}(t)$  are elaborated by a secondary fully connect layer  $f_{c_k}$  with  $k = 1$  to predict the next action  $\mathbf{y}_{next}$ . This is possible since the vector  $\mathbf{w}(t)$  keeps both the

information of the current input  $X(t)$  (see eq. 2) and the information of the previous actions, due to the interaction between the memory and  $q_2$ . The current action classification vector adds up these information to predict the next action:

$$\mathbf{y}_{next}(t) = \sigma(f_{C_k}([\max(0, \mathbf{w}(t) + \mathbf{b}_{next}), \mathbf{y}_{now}(t)])) \quad (11)$$

To speed up the contribution of the convolutional layers of  $q_0$  to the optimization, we define a loss function taking into account a direct  $M(t)$  classification (see eq. 5):

$$\mathbf{aux}(t) = \sigma(f_{C_k}(M(t))) \quad (12)$$

Here  $f_{C_k}$  is a fully connected layer with  $k = 3$ .

Having defined the output of AFN we illustrate the cross entropy loss function on the three outputs, namely  $\mathcal{L}_1$  on  $\mathbf{y}_{now}$ ,  $\mathcal{L}_2$  on  $\mathbf{y}_{next}$  and  $\mathcal{L}_3$  on  $\mathbf{aux}$ .

$$\mathcal{L}_1(t) = - \sum_i \bar{y}_i(t) \log(y_{now_i}(t)) \quad (13)$$

$$\mathcal{L}_2(t) = - \sum_i \hat{y}_i(t) \log(y_{next_i}(t)) \quad (14)$$

$$\mathcal{L}_3(t) = - \sum_i \bar{y}_i(t) \log(aux_i(t)) \quad (15)$$

Here  $\bar{y}$  and  $\hat{y}$  are the target vectors, respectively for the current action and the next, and  $i$  is the  $i$ -th element of the corresponding vector. The total loss is obtained by combining the above loss function as follow:

$$\mathcal{L}_{tot}(t) = \alpha(t^*)((1 - \beta(t^*))\mathcal{L}_1(t) + \beta(t^*)\mathcal{L}_2(t)) + (1 - \alpha(t^*))\mathcal{L}_3(t) \quad (16)$$

Here  $t^*$  is the previous training step,  $\alpha$  is the accuracy measured on the auxiliary classification  $\mathbf{aux}$ , and  $\beta$  is the accuracy computed on the current classification  $\mathbf{y}_{now}$ . The accuracy parameters  $\alpha$  and  $\beta$  combine  $\mathcal{L}_1$ ,  $\mathcal{L}_2$  and  $\mathcal{L}_3$  dynamically, according to the performances reached by the network at the previous training step  $t^*$ . The following equation illustrates how  $\mathcal{L}_{tot}$  changes in four key steps of the training process, where  $\epsilon$  is a small positive value:

$$\mathcal{L}_{tot}(t) = \begin{cases} \mathcal{L}_3(t) & \text{if } \alpha \in [0, \epsilon] \text{ and } \beta \in [0, \epsilon] \\ \frac{1}{2}(\mathcal{L}_1(t) + \mathcal{L}_3(t)) & \text{if } \alpha \in [\frac{1}{2} - \epsilon, \frac{1}{2} + \epsilon] \text{ and } \beta \in [0, \epsilon] \\ \frac{1}{2}(\mathcal{L}_2(t) + \mathcal{L}_1(t)) & \text{if } \alpha \in [1 - \epsilon, 1] \text{ and } \beta \in [\frac{1}{2} - \epsilon, \frac{1}{2} + \epsilon] \\ \mathcal{L}_2(t) & \text{if } \alpha \in [1 - \epsilon, 1] \text{ and } \beta \in [1 - \epsilon, 1] \end{cases} \quad (17)$$

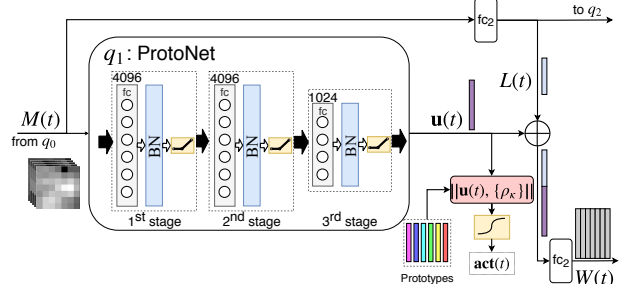


Figure 4: Prototypical Network for activity classification and advising.

The parameters  $\alpha$  and  $\beta$  in eq. 16 enforce the optimization of the convolution component  $q_0$  in the early training steps, when both  $\alpha$  and  $\beta$  are close to  $\epsilon$  (first line in eq. 17). On the other hand as they both reach max values (last line in eq. 17), they push the optimization toward  $\mathbf{y}_{next}$ . In the intermediate steps (second and third line in eq. 17)  $\alpha$  and  $\beta$  favor the optimization of  $\mathbf{y}_{now}$ . Clearly, the transitions among these steps are smooth and we can note that  $\mathcal{L}_3$  optimization is gradually ignored as  $\alpha$  increases. Similarly,  $\mathcal{L}_1$  optimization is steadily disregarded as soon as  $\beta$  increases. The graph in Figure 3 illustrates the above considerations.

#### 4.4 Activities embedding

The  $q_1$  component of AFN is an activity encoder which produces an embedding representative of the activity performed. The produced embedding provides an essential context for forecasting the action that follows by predicting the activity class the observed tensor belongs to.

In order to make the network learn a representative embedding, we consider a Prototypical Network (ProtoNet) [38] comprising three stages each formed by a fully connected layer, a batch normalization layer and a ReLU activation function (see Figure 4). The fully connected layers are of size 4096, 4096 and 1024, respectively. The network receives sample tensors  $M(t)$  from  $q_0$  and predicts the activity which contextualizes the performed actions via the embedding described below.

The input batch contains  $\xi$  videos corresponding to  $K$  activities. Reintroducing the indices used in §4.1, we define  $\mathcal{M}_j = \{M_{j,1}, \dots, M_{j,\zeta}\}$  as a collection of feature tensors corresponding to the  $\zeta$  samples of activity  $A_j$  contained in the batch. Similarly to [38], we assume that there exists a latent space where the embedded vectors  $\mathbf{u} = f_\theta(M)$ , with  $M \in \mathcal{M}_j$ , cluster around the corresponding activity prototype  $\rho_j$ . In our context, letting  $\theta$  be the parameters of component  $q_1$ , the network training approximates this optimal embedding function  $f_\theta(\cdot)$ . In this way,  $q_1$  is used to compute embedded vectors which contain context about the performed activity and therefore provide advised informa-

tion for forecasting the next action.

Specifically, two disjoint subsets  $C_j$  and  $Q_j$  are sampled randomly from the collection  $\mathcal{M}_j$ . Letting  $|C_j|$  denote the cardinality of  $C_j$ , the prototype of activity  $A_j$  is defined as the sample mean of the embedded vectors corresponding to the samples contained in  $C_j$ , namely

$$\rho_j = \frac{1}{|C_j|} \sum_{M \in C_j} f_\theta(M). \quad (18)$$

The likelihood of an instance  $M_q \in Q_j$  belonging to activity  $j$  is then given by

$$p(j|M_q, \theta) = \frac{\gamma_j \exp(-\|f_\theta(M_q) - \rho_j\|)}{\sum_{\kappa} \gamma_{\kappa} \exp(-\|f_\theta(M_q) - \rho_{\kappa}\|)}. \quad (19)$$

Here,  $\gamma_j$  are learnable parameters that represent the relative weight of each activity cluster in the latent space.

Considering now that the class of  $M_q$  is  $j$ , the parameters  $\theta$  are computed via Stochastic Gradient Descent by minimizing the loss

$$\mathcal{L}_{act} = \sum_{j=1}^K \sum_{M \in Q_j} \left\{ \|f_\theta(M) - \rho_j\| - \log \gamma_j + \log \left( \sum_{\kappa} \gamma_{\kappa} \exp(-\|f_\theta(M) - \rho_{\kappa}\|) \right) \right\}, \quad (20)$$

which corresponds to the negative log of (19) over the batch.

The latent vector  $\mathbf{u} = f_\theta(M)$  computed by the ProtoNet is then concatenated to the output of  $f_{c_2}$ , according to eq. 8, to provide context for forecasting the next action.

## 5 Results

**Overview.** By action *anticipation* we intend action labeling given just a few observed frames. Slightly differently from the literature (e.g. [33]) AFN samples 6 frames, out of a second, at any point in a video, not just at the beginning of the action. In fact, we do not rely on one shot actions nor on trimming at inference time. In other words, we consider videos of any length without taking into account actions start and end. By action *forecasting*, we intend labeling an action when no frames have been yet observed, and only the previous action has been anticipated, according to the above definition of *anticipation*. Figure 5 illustrates anticipation and forecasting.

We consider two types of activities, according to the datasets taken into account (see next paragraph). The first type, used for anticipation, collects activities not further subdivided into action sequences. The second type, suitable for forecasting future actions, is split into actions forming sequences, which can be represented as directed (not

acyclic) graphs. Because AFN both anticipates and forecasts the next action, to confront with the state of the art we take into account both dataset types, in so showing the extreme flexibility of its architecture.

### 5.1 Datasets Selection

For *action anticipation* we have selected the two datasets common to most of the recent works on early action recognition, namely **JHMDB** and **UCF101** datasets. JHMDB [11] is composed by 928 videos of 21 selected actions out of the 51 of the original HMDB [21]. **UCF101** [39] has 101 action categories for 430 hours of videos.

Experiments on *action forecasting*, are done on four datasets: **Breakfast** [20], **Charades** [35], **CAD120** [18] and **MPII cooking dataset** [30].

The Breakfast [20] dataset has 10 activity categories over 48 actions. The dataset consists of 712 videos taken by 52 different actors. Charades dataset [35] combines 40 objects and 30 actions in 15 scenes generating a number of 157 action classes for 9848 videos. To experiment on Charades dataset, we defined the contexts as the activities, slightly modifying the temporal annotations, since we do not consider objects. For example, living-room-activity collects the actions performed in a living room.

MPII cooking activities dataset [30] has 65 action classes for 14 dishes preparation activities, performed by 12 participants. There are 44 videos for about 8 hours of videos.

### 5.2 Implementation Details

The whole set of experiments has been performed on two computers, both equipped with an i9 Intel processor and 128GB of RAM, and with 4 NVIDIA Titan V. AFN is developed using Tensorflow 1.11.

**Protocols** For training and testing our system, we used in turn all the datasets, fixing 60% for training, 30% for testing and 10% for validation, where not already defined by the dataset. We did not select the actors to separate training, validation and test, since in some datasets not all actions are performed by each actor. For optimization we used Adam [13] and gradient clipped to 1. We trained the model with different batch sizes, mainly to cope with the ProtoNet component of the network,  $q_1$ . The final size was 25, due to the large tensors (see eq. 2). The image size at input is  $112 \times 112$ . We used a dynamic learning rate, starting with  $10^{-4}$ , decreasing it of a factor of 0.9 every  $3k$  steps. We used dropout 0.6 only at the convolutional layers of  $q_0$ . The training speed is roughly 11 steps per sec. Having 45 Epochs, each of  $10k$  steps, the overall training time is about  $43k$  seconds.



Figure 5: The schema illustrates the effects of sampling 6 frames from 1 sec. at any point in a video, at inference time. The general idea is shown in the first strip: anticipation here is 3.3% of the action *pour coffee* and the next action is predicted 30 sec. in advance. Below, we observe two cases that might occur when jumping into a video at a random time point, here 72.28 sec. after the video start. In the second strip, the current action *smear butter* is anticipated, and the next action *take topping* starting 56 sec. after it, is forecast. In the third stripe, the sample is taken on an interval overlapping *smear butter* and *take topping*, in this case neither anticipation nor forecasting occurs. Details are given in §5.4.

### 5.3 Comparison with the State-of-the-Art

The comparison with the state of the art has been done for both anticipation and forecasting. Note that, as AFN uses softmax, accuracy is simply frequency count of correct predictions out of all predictions. In order to make the confrontation as fair as possible for all the works taken into account, we have considered different measures for both anticipation and forecasting.

**Action anticipation** For action anticipation we considered the datasets JHMDB [11] and UCF101[39] as discussed in §5.1. Results are shown in Table 1. Anticipation values are defined as:

$$\Delta^- = 1/\mu_\ell(V) \quad (21)$$

where  $\Delta^- \in \{0.1, 0.2, 0.5\}$  is the anticipation value and  $\mu_\ell(V)$  is the mean length of selected video  $V$ , for the specific dataset. In this way, we can relate the anticipation values chosen by the cited authors with our fixed anticipation value of 1 sec., which is independent of the video length. Video length is shown in the first column, anticipation time in the second column. Footnotes in the table specify the number of activities in the dataset considered by the cited approach. In bold are the best in class. We can see that AFN outperforms all the approaches on anticipation, according to the displayed measure.

**Action forecasting** Here we compare with two methods: [6] on the Breakfast dataset, and [27] on the MPII dataset. No works on action forecasting are based on the Charades and CAD120 datasets, as far as we know. Table 2 confronts with [6] and both Table 3 and Table 4 with [27]. To com-

pare with Farha *et Al.* [6] on the Breakfast dataset we consider the 20% and the 30% of the video length as observation. This given we forecast over an horizon of 10% of the remaining video. The comparison takes into account both the RNN-based anticipation and the CNN-based anticipation proposed in [6]. We have chosen these forecasting measures, since we forecast precisely the next action, while [6] forecast all actions up to the video end. Though this is done at the cost of an accuracy significantly lower than ours, as the table shows.

Comparisons with [27] are shown in Table 3 and in Table 4. In Table 3 we compare precision and recall with respect to next action forecasting, considering only the top 1. In Table 4, on the other hand, we compare the accuracy with respect to the number of past recognized actions. We observe that the improvement is between 11% and 13% percent in the first comparison and from about 6% up to 17% in the second comparison, as as the past sequence length increases.

### 5.4 Evaluation of AFN

We evaluate AFN specifically on next action forecasting, since for anticipation all the datasets considered are covered in Table 1. The confusion matrix shown in Figure 6 shows the average accuracy of actions occurring in activities, for Breakfast dataset. In Table 6 we show the accuracy for next action forecasting when jumping into an activity video sequence. We consider four cases: 1) at the beginning of an action, namely when the timeline horizon to the next action

Table 1: Comparison on Anticipation

UCF101			
Video length	%	Framework	Accuracy
2s	0.5	mem-LSTM [16]	83.37%
		DeepSCN [17]	85.46%
		A+AF [37] <sup>a</sup>	~ 87%
		fm+RBF+GAN+Inception V3 [33] <sup>a</sup>	98.00%
		global-local LSTM [22] <sup>b</sup>	74.30%
		Two-Stream Network [22] <sup>b</sup>	90.50%
		<b>AFN</b>	<b>98.30%</b>
5s	0.2	global-local LSTM [22] <sup>b</sup>	70.20%
		Two-Stream Network [22] <sup>b</sup>	89.3%
		A+AF[37] <sup>a</sup>	~ 83%
		<b>AFN</b>	<b>93.73%</b>
10s	0.1	global-local LSTM [22] <sup>b</sup>	68.50%
		Two-Stream Network [22] <sup>b</sup>	87.5%
		Static and Dynamic CNN [29] <sup>a</sup>	89.30%
		DeepSCN [17]	44.31 %
		mem-LSTM [16]	51.02%
		RED [7]	37.5%
		Deep K-3 [42]	43.6%
		<b>AFN</b>	<b>91.23%</b>
JHMDB			
2s	0.5	TP Net [36] <sup>c</sup>	74.1%
		Multi-Stage LSTM [1]	58.0%
		A+AF [37]	~ 63%
		<b>AFN</b>	<b>85.4%</b>
5s	0.2	Static and Dynamic CNN [29]	61.0%
		TP Net [36]	74.8%
		Multi-Stage LSTM [1]	55.0%
		A+AF[37]	~ 60%
		fm+RBF+GAN+Inception V3 [33]	73%
		<b>AFN</b>	<b>81.6%</b>

<sup>a</sup>UCF101 (24 actions)<sup>b</sup>UCF11<sup>c</sup>It uses atomic actions

Table 2: Comparison on Action Forecasting

Prediction Observation	10% (Next Action)	
	20%	30%
RNN-based Anticipation [6]	18.11%	21.64%
RNN-based Anticipation (Ground Truth given) [6]	60.35%	61.45%
CNN-based Anticipation [6]	17.90%	22.44%
CNN-based Anticipation (Ground Truth given) [6]	57.97%	60.32%
<b>AFN</b>	<b>91.09%</b>	<b>93.27%</b>

is between 90% and 100%, 2) after the 90% but before the middle of the action; 3) after the middle, before the last 1%, and 4) at the end of the current action. We can see that the accuracy of the prediction does not significantly improve with respect to the distance from next action. On the other hand the accuracy drops to zero when the selected sample is

Table 3: Comparison on next Action Forecasting I

MPII Cooking Dataset			
Framework	Precision	Recall	Accuracy (Top-1)
Activity Label Prediction [27]	70.7%	66.5%	80.1%
<b>AFN</b>	<b>78.5%</b>	<b>74.6%</b>	<b>86.2%</b>

Table 4: Comparison on next Action Forecasting II

Framework	Sequence length 2	Sequence length 3	Sequence length 5	Sequence length 7	Sequence length 9
ALP [27]	78.8%	80.1%	79.2%	77.8%	77.2%
<b>AFN</b>	<b>89.6%</b>	<b>92.7%</b>	<b>92.8%</b>	<b>93.3%</b>	<b>94.1%</b>

Table 5: Ablation with respect to next action forecasting

Removed Component	Dataset	Current Action Accuracy	Next Action Accuracy
$q_1$	Breakfast	85.06%	80.54%
	Charades	81.23%	78.65%
	CAD-120	82.34%	79.89%
$q_4$	Breakfast	87.74%	—
	Charades	84.34%	—
	CAD-120	84.75%	—
$\mathcal{L}_3$	Breakfast	79.12%	76.23%
	Charades	75.59%	71.98%
	CAD-120	77.03%	74.29%

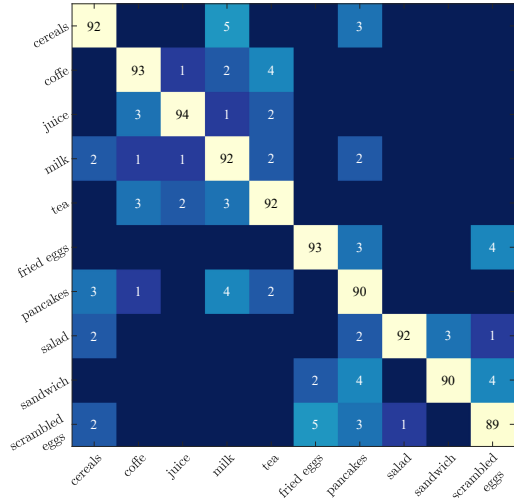


Figure 6: Confusion matrix for the Activities in Breakfast. Values less than 1 are dropped.

in between the current and next action, since AFN discards these cases, see also Figure 5. The best dataset for our experiments turns out to be Breakfast. Ablation experiments are shown in Table 5. Here, we can observe the accuracy of AFN when, in turn, the components  $q_1$ ,  $q_4$ , and the auxiliary connection to the convolutional layers of  $q_0$ , indicated



in the table by  $\mathcal{L}_3$ , are removed.

Table 6: Evaluation of AFN for next action forecasting

Dataset	Accuracy % according to timeline horizon $h$ % to next action			
	90% ≤ $h$ < 100%	50% ≤ $h$ < 90%	1% ≤ $h$ < 50%	0% ≤ $h$ < 1%
MPII [30]	93.4%	93.7%	93.9%	0%
Breakfast [20]	<b>94.2%</b>	<b>94.6%</b>	<b>94.72%</b>	0%
Charades [35]	89.5%	89.8%	90.11%	0%
CAD120 [18]	92.6%	93.2%	93.5%	0%

More results are shown in the supplementary materials.

## References

- [1] M. S. Aliakbarian, F. Saleh, M. Salzmann, B. Fernando, L. Petersson, and L. Andersson. Encouraging lstms to anticipate actions very early. *(ICCV)*, 2017. **3, 8**
- [2] J. Bütepage, M. J. Black, D. Kragic, and H. Kjellström. Deep representation learning for human motion prediction and classification. In *(CVPR)*, 2017. **2**
- [3] Z. Cao, T. Simon, S.-E. Wei, and Y. Sheikh. Realtime multi-person 2d pose estimation using part affinity fields. In *(CVPR)*, 2017. **3**
- [4] A. Chakraborty and A. K. Roy-Chowdhury. Context-aware activity forecasting. In *(ACCV)*, 2014. **3**
- [5] D. Damen, H. Doughy, G. M. Farinella, S. Fidler, A. Furnari, E. Kazakos, D. Moltisanti, J. Munro, T. Perrett, W. Price, et al. Scaling egocentric vision: The epic-kitchens dataset. In *(ECCV)*, 2018. **2**
- [6] Y. A. Farha, A. Richard, and J. Gall. When will you do what?-anticipating temporal occurrences of activities. In *(CVPR)*, 2018. **1, 3, 7, 8**
- [7] J. Gao, Z. Yang, and R. Nevatia. Red: Reinforced encoder-decoder networks for action anticipation. In *(BMVC)*, 2017. **1, 3, 8**
- [8] K. P. Hawkins, S. Bansal, N. N. Vo, and A. F. Bobick. Anticipating human actions for collaboration in the presence of task and sensor uncertainty. In *(ICRA)*, 2014. **1**
- [9] S. Hochreiter and J. Schmidhuber. Long short-term memory. *Neural computation*, 9(8):1735–1780, 1997. **4**
- [10] A. Jain, A. R. Zamir, S. Savarese, and A. Saxena. Structural-rnn: Deep learning on spatio-temporal graphs. In *(CVPR)*, 2016. **2**
- [11] H. Jhuang, J. Gall, S. Zuffi, C. Schmid, and M. J. Black. Towards understanding action recognition. In *(ICCV)*, 2013. **2, 6, 7**
- [12] A. Karpathy, G. Toderici, S. Shetty, T. Leung, R. Sukthankar, and L. Fei-Fei. Large-scale video classification with convolutional neural networks. In *(CVPR)*, 2014. **3**
- [13] D. P. Kingma and J. Ba. Adam: A method for stochastic optimization. *arXiv:1412.6980*, 2014. **6**
- [14] K. M. Kitani, B. D. Ziebart, J. A. Bagnell, and M. Hebert. Activity forecasting. In *(ECCV)*, 2012. **1, 2**
- [15] Y. Kong and Y. Fu. Human action recognition and prediction: A survey. *arXiv:1806.11230*, 2018. **2**
- [16] Y. Kong, S. Gao, B. Sun, and Y. Fu. Action prediction from videos via memorizing hard-to-predict samples. In *(AAAI)*, 2018. **2, 8**
- [17] Y. Kong, Z. Tao, and Y. Fu. Deep sequential context networks for action prediction. In *(CVPR)*, 2017. **8**
- [18] H. S. Koppula, R. Gupta, and A. Saxena. Learning human activities and object affordances from rgb-d videos. *(IJRR)*, 32(8):951–970, 2013. **2, 6, 9**
- [19] H. S. Koppula and A. Saxena. Anticipating human activities using object affordances for reactive robotic response. *(TPAMI)*, 38(1):14–29, 2016. **1**
- [20] H. Kuehne, A. B. Arslan, and T. Serre. The language of actions: Recovering the syntax and semantics of goal-directed human activities. In *(CVPR)*, 2014. **2, 3, 6, 9**
- [21] H. Kuehne, H. Jhuang, E. Garrote, T. Poggio, and T. Serre. Hmdb: a large video database for human motion recognition. In *(ICCV)*, 2011. **6**
- [22] S. Lai, W.-S. Zheng, J.-F. Hu, and J. Zhang. Global-local temporal saliency action prediction. *Trans. on Image Proc.*, 27(5):2272–2285, 2018. **3, 8**
- [23] T. Lan, T.-C. Chen, and S. Savarese. A hierarchical representation for future action prediction. In *(ECCV)*, 2014. **1, 2, 3**
- [24] X. Liang, L. Lee, W. Dai, and E. P. Xing. Dual motion gan for future-flow embedded video prediction. In *(ICCV)*, 2017. **1**
- [25] J. Liu, J. Luo, and M. Shah. Recognizing realistic actions from videos "in the wild". In *(CVPR)*, 2009. **3**
- [26] S. Ma, L. Sigal, and S. Sclaroff. Learning activity progression in lstms for activity detection and early detection. In *(CVPR)*, 2016. **1**
- [27] T. Mahmud, M. Hasan, and A. K. Roy-Chowdhury. Joint prediction of activity labels and starting times in untrimmed videos. In *(ICCV)*, 2017. **3, 7, 8**
- [28] S. Oh, A. Hoogs, A. Perera, N. Cuntoor, C.-C. Chen, J. T. Lee, S. Mukherjee, J. Aggarwal, H. Lee, L. Davis, et al. A large-scale benchmark dataset for event recognition in surveillance video. In *(CVPR)*, 2011. **3**
- [29] C. Rodriguez, B. Fernando, and H. Li. Action anticipation by predicting future dynamic images. *arXiv:1808.00141*, 2018. **2, 8**
- [30] M. Rohrbach, S. Amin, M. Andriluka, and B. Schiele. A database for fine grained activity detection of cooking activities. In *(CVPR)*, 2012. **2, 3, 6, 9**
- [31] M. S. Ryoo. Human activity prediction: Early recognition of ongoing activities from streaming videos. In *(ICCV)*, 2011. **2**
- [32] M. S. Ryoo and J. K. Aggarwal. UT-Interaction Dataset, ICPR contest on Semantic Description of Human Activities (SDHA). [http://cvrc.ece.utexas.edu/SDHA2010/Human\\_Interaction.html](http://cvrc.ece.utexas.edu/SDHA2010/Human_Interaction.html), 2010. **2**
- [33] Y. Shi, B. Fernando, and R. Hartley. Action anticipation with rbf kernelized feature mapping rnn. In *(ECCV)*, 2018. **1, 3, 6, 8**
- [34] G. A. Sigurdsson, A. Gupta, C. Schmid, A. Farhadi, and K. Alahari. Actor and observer: Joint modeling of first and third-person videos. In *(CVPR)*, 2018. **2**

- [35] G. A. Sigurdsson, G. Varol, X. Wang, A. Farhadi, I. Laptev, and A. Gupta. Hollywood in homes: Crowdsourcing data collection for activity understanding. In *(ECCV)*, 2016. 2, 3, 6, 9
- [36] G. Singh, S. Saha, and F. Cuzzolin. Predicting action tubes. *arXiv:1808.07712*, 2018. 2, 3, 8
- [37] G. Singh, S. Saha, M. Sapienza, P. H. Torr, and F. Cuzzolin. Online real-time multiple spatiotemporal action localisation and prediction. In *(ICCV)*, 2017. 2, 8
- [38] J. Snell, K. Swersky, and R. Zemel. Prototypical networks for few-shot learning. In I. Guyon, U. V. Luxburg, S. Bengio, H. Wallach, R. Fergus, S. Vishwanathan, and R. Garnett, editors, *In (NIPS)*. 2017. 2, 5
- [39] K. Soomro, A. Roshan Zamir, and M. Shah. UCF101: A dataset of 101 human actions classes from videos in the wild. In *(CRCV-TR-12-01)*, 2012. 2, 6, 7
- [40] S. Stein and S. J. McKenna. Combining embedded accelerometers with computer vision for recognizing food preparation activities. In *(ACM Int. Conf. on Pervasive and Ubiquitous Computing)*, 2013. 3
- [41] D. Tran, L. Bourdev, R. Fergus, L. Torresani, and M. Paluri. Learning spatiotemporal features with 3d convolutional networks. In *(ICCV)*, 2015. 4
- [42] C. Vondrick, H. Pirsivash, and A. Torralba. Anticipating visual representations from unlabeled video. In *(CVPR)*, 2016. 1, 2, 8
- [43] C. Vondrick and A. Torralba. Generating the future with adversarial transformers. In *(CVPR)*, 2017. 2, 3
- [44] J. Walker, C. Doersch, A. Gupta, and M. Hebert. An uncertain future: Forecasting from static images using variational autoencoders. In *(ECCV)*, 2016. 1
- [45] Y. Xu, Z. Piao, and S. Gao. Encoding crowd interaction with deep neural network for pedestrian trajectory prediction. In *(CVPR)*, 2018. 2
- [46] K.-H. Zeng, W. B. Shen, D.-A. Huang, M. Sun, and J. C. Niebles. Visual forecasting by imitating dynamics in natural sequences. In *(ICCV)*, 2017. 1

# Supplementary Material

## 1 Next action label

In this supplementary material we provide an evaluation for the proposed next action forecasting framework. In particular, we present confusion matrices for the datasets Charades, Breakfast, CAD120 and MPII-kitchen. We also provide an accuracy according to the time distance between the anticipation of the current action and the starting time of the next action (see also Table 6 in the paper). To produce the confusion matrices we specifically recorded the false positives. For true and false negatives we considered the “action” *null* in CAD120, the *background* in the dataset MPII-Kitchen, denoting when no activity is detected. Similarly for the dataset Breakfast we considered the *SIL* action specifying the start and end of an action.

The *time to next action* accuracy graph shows the time left to the next action start. To illustrate this accuracy value we have selected actions from the datasets with highest time variance defined as follows. Let  $S$  be the set of reference (the test set),  $A(t)$  be the label of an action, and let  $\Delta A(t) = A'(t) - A(t^+)$ , with  $A'$  a label of any of the actions following  $A$  in the set considered, and  $(t^+)$  the second at which  $A$  is anticipated. Let  $\mu_A = \frac{1}{N} \sum_{i=1}^N \Delta A(t_i)$  with  $A(t_i)$  the same action  $A$  with  $t_i$  varying in all occurrence of  $A \in S$ . We say that  $A$  has a high variation (with respect to forecasting and anticipation) if  $\mu_A/\mu_B > \lambda$  for some  $\lambda$  experimentally established for each set, and for a number of other actions  $B$  in  $S$  (where the number depends on  $\lambda$ ). When  $\Delta A(t)$  is negative then there is no next action  $A'$ . This variation is relevant because it shows if accuracy in forecasting is independent of the subject performing an action and the circumstances in which it is performed. All evaluations are done on the test sets.

### 1.1 CAD120 Dataset

CAD120 dataset [1] has 120 videos annotated with 10 actions and 10 high-level activities. Note that the actions are the same for all the activities. This is particularly interesting for the ProtoNet component of AFN, thus we show also the confusion matrix for the activities of CAD120.

Figure 1 shows on the left the confusion matrix, including the *null* action and on the right it shows the classification by the ProtoNet component of AFN. Figure 2 shows the next action forecasting accuracy with respect to the time

distance between the current action anticipation and the next action start. Here we considered all the actions.

### 1.2 MPII-cooking dataset

The MPII cooking activities [3] dataset consists of 65 actions recorded from 12 subjects.

For this dataset there are 44 videos at high resolution, with a framerate of 29.4hz. The confusion matrix for the next activity prediction is illustrated in Figure 3. True positive are illustrated with a jet map and small digits indicate the accuracy of correct predictions. In white the false positive. To record false negatives we used the fictitious action *background* included in the dataset annotations.

Figure 4 shows the accuracy of next action forecasting according to the time distance between the first second of the current action to the start point of the next action. We considered the 23 actions, of the 65 ones, with highest variation for  $\lambda = 2$ . Videos in MPII dataset are acquired at 29.4Hz. According to the framerate there is a 1% of cases in which the time lapse between the current-action-start and the next-action-start is less than a second, this 1% is collected as an error for AFN.

### 1.3 Breakfast Dataset

The Breakfast dataset [2], in its rough version has 48 actions occurring in 10 activities (see Figure 6 in the submitted paper). Figure 5 shows the complete confusion matrix, including the *SIL* operator, considered for recording false negative. For breakfast it amounts to forecast the existence of a next action, while the activity should have been concluded.

In Breakfast dataset, framerate is 15Hz, and the time lapse between the current action anticipation and the next action start has a mean value of 5.1 seconds. On the other hand a less than a second time lapse between the current action start and the next action start occurs only in 4% of all the videos (77 hours of videos). We consider this amount an error for our framework. As we did for MPII-kitchen also in this case we considered the actions with highest variance to evaluate the accuracy on the time distance with respect to the next action start, here we choose  $\lambda = 0.82$ . Accuracy for time distance is illustrated in Figure 6.

## 1.4 Charades Dataset

The Charades dataset [4] is a very rich dataset with 157 action classes, objects, affordances and descriptions. Because all actions are specified with respect to a context scene we considered the context scenes as the high level activities for the ProtoNet. Each video has on average 6.8 actions and several actions are considered co-occurring, such as closing-opening a window, so to obtain a sequence we had to adapt the time intervals. For Charades we used the proposed separation in training and test. Figure 7 shows the confusion matrix for a subset of 48 actions for visibility reasons (chosen randomly over the set of 156 actions). For an action sequence completion we have added an *end*, not shown in the confusion matrix.

Similarly, we have chosen a  $\lambda = 0.94$  to analyze the accuracy with respect to time distance to next action, illustrated in Figure 8.

## References

- [1] H. S. Koppula, R. Gupta, and A. Saxena. Learning human activities and object affordances from rgb-d videos. (*IJRR*), 32(8):951–970, 2013. 1
- [2] H. Kuehne, A. B. Arslan, and T. Serre. The language of actions: Recovering the syntax and semantics of goal-directed human activities. In (*CVPR*), 2014. 1
- [3] M. Rohrbach, S. Amin, M. Andriluka, and B. Schiele. A database for fine grained activity detection of cooking activities. In (*CVPR*), 2012. 1
- [4] G. A. Sigurdsson, A. Gupta, C. Schmid, A. Farhadi, and K. Alahari. Actor and observer: Joint modeling of first and third-person videos. In (*CVPR*), 2018. 2

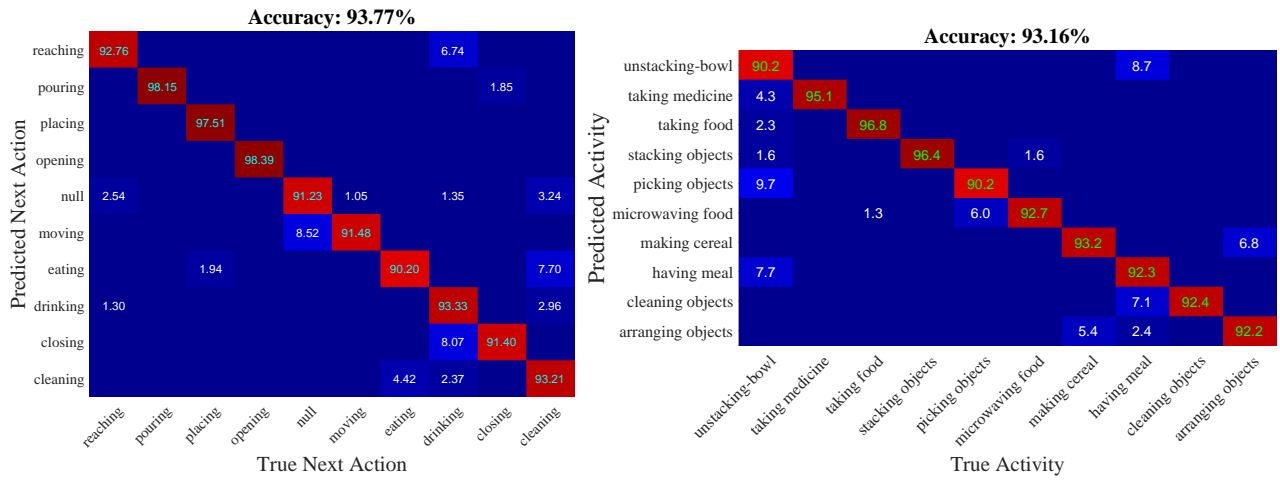


Figure 1: On the left the Confusion Matrix for CAD120 dataset. Values less than 0.8 are not shown, the heat color-map is *jet*. The *null* action is recorded to show false negatives. On the right Confusion Matrix for CAD120 Activities.

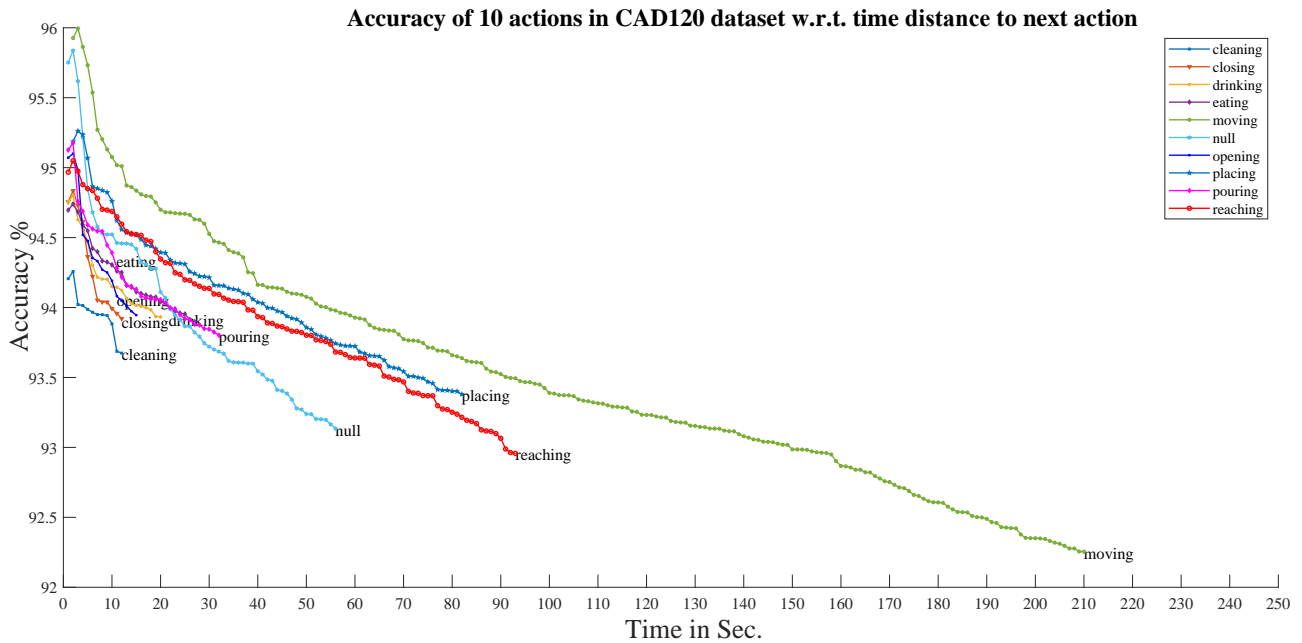


Figure 2: Accuracy with respect to time distance between current action anticipation to next action start for dataset CAD120. Time is computed according to videos framerate.

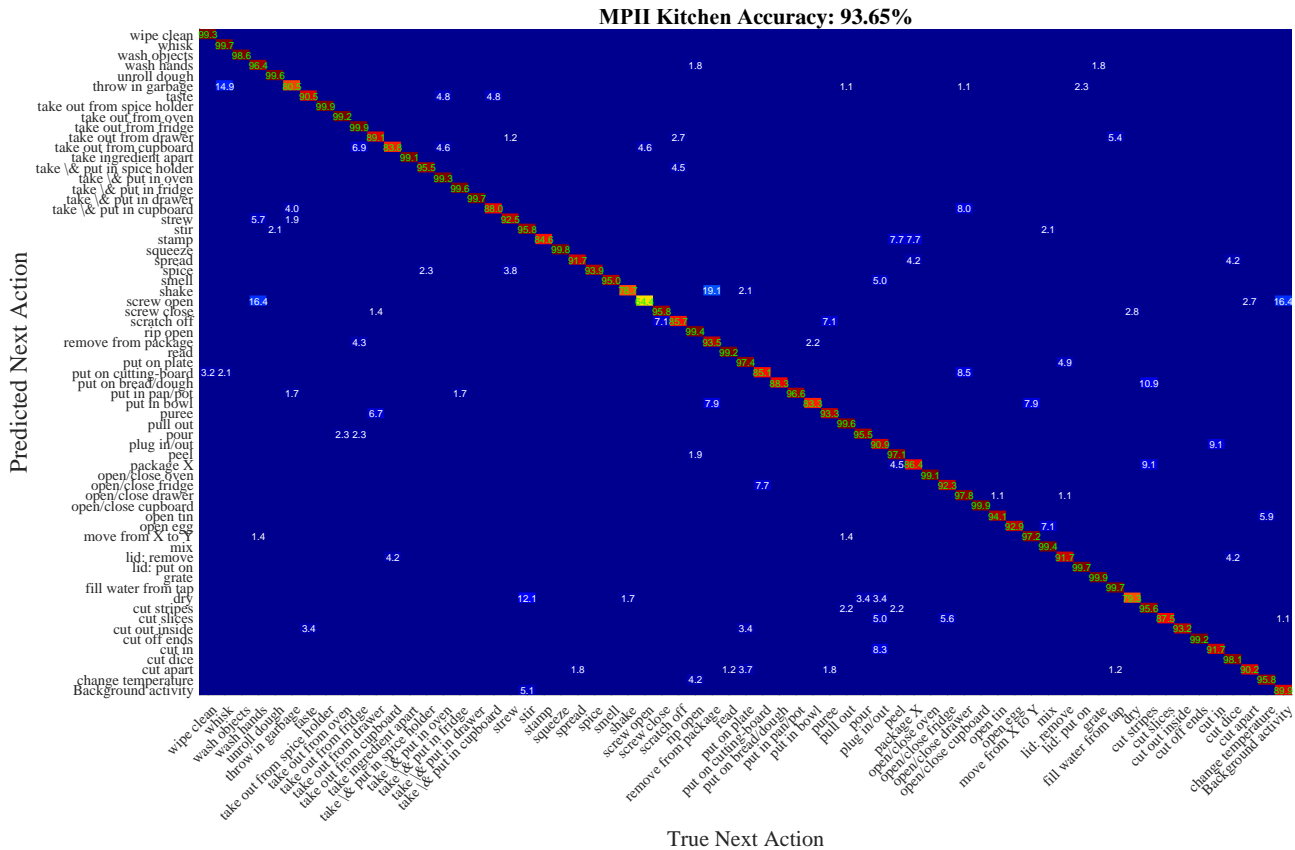


Figure 3: Confusion matrix for the MPII-kitchen dataset. The heat-map is *jet*, values less than 1 are not shown.

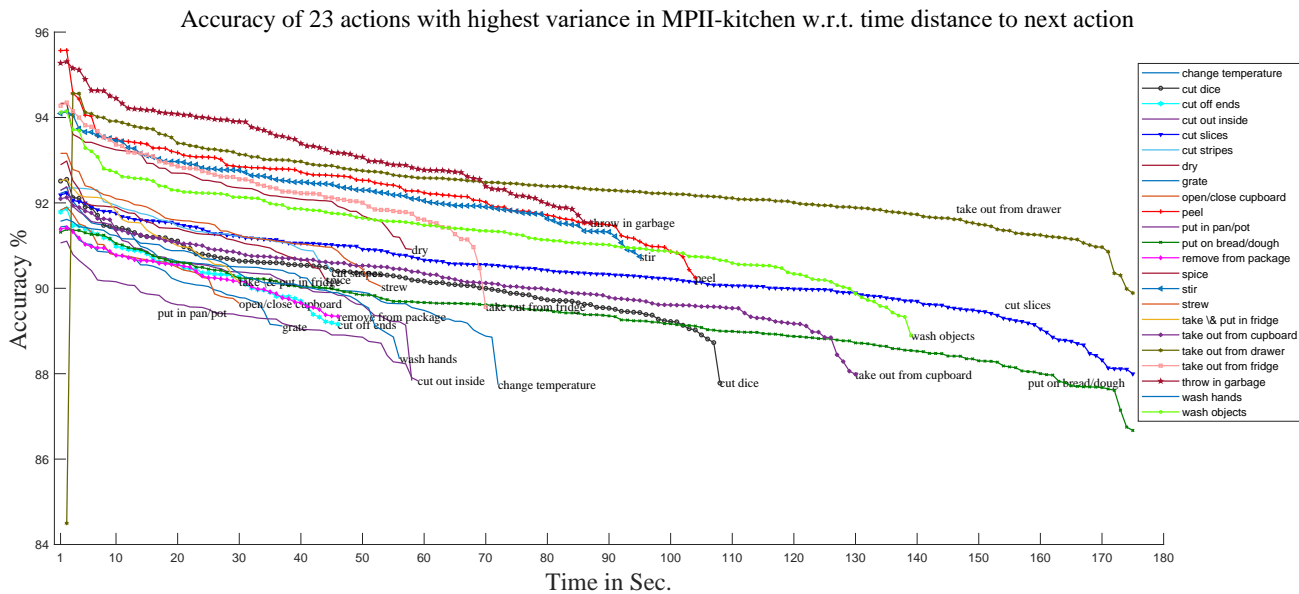


Figure 4: Accuracy trends for next action prediction for MPII-kitchen dataset, considering the 23 actions with greatest variance over the 64 in the dataset. The time line indicates the time distance to the next action, for each occurrence of the indicated action, in the video dataset. Framerate is 29.4Hz

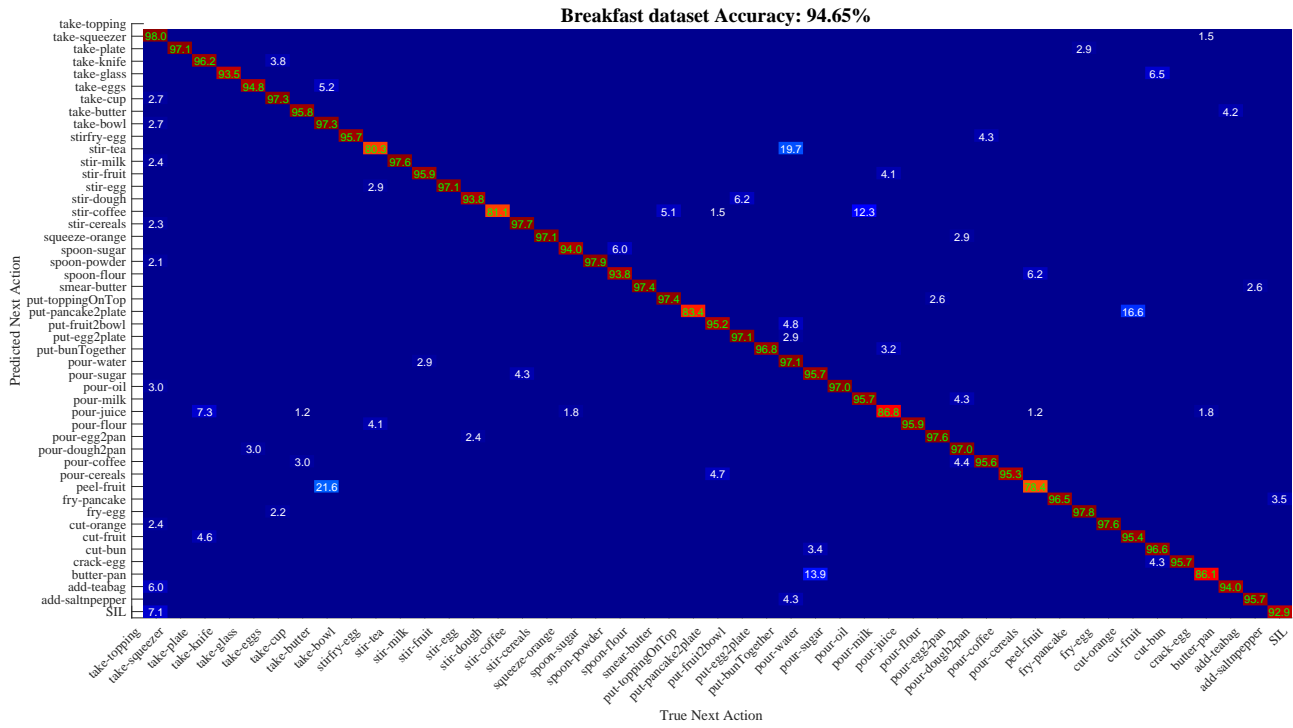


Figure 5: Confusion matrix for the Breakfast dataset. The heat-map is *jet*, values less than 1 are not shown. The *SIL* actions is recorded for false negatives.

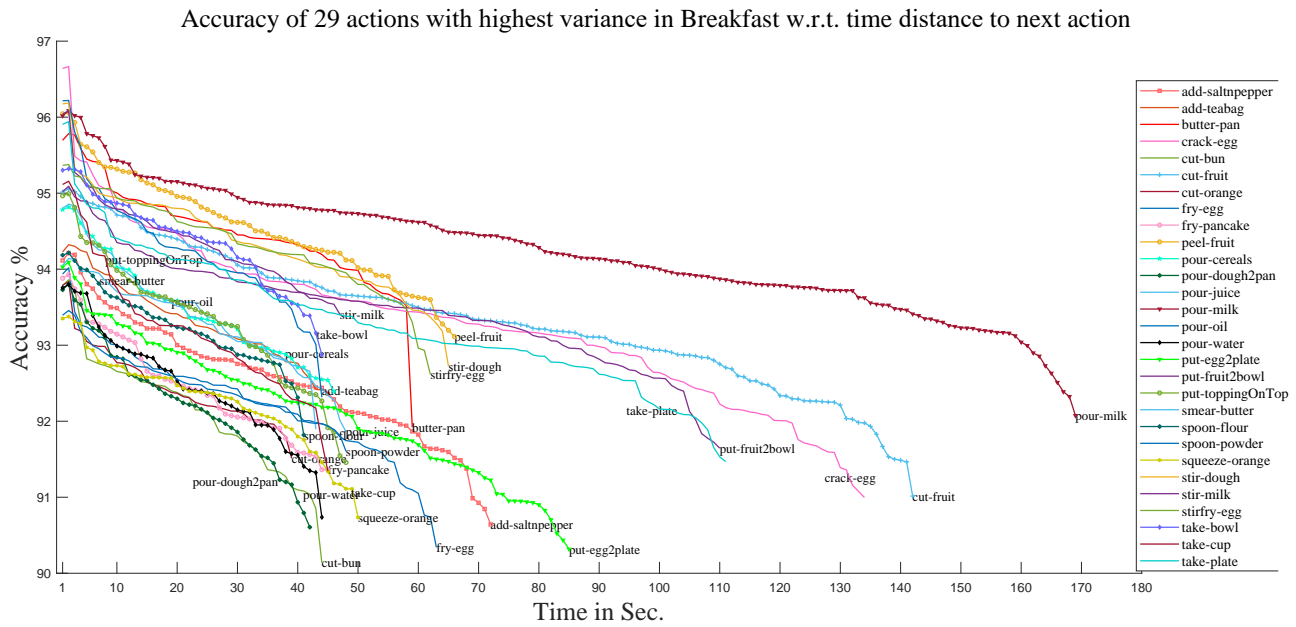


Figure 6: Accuracy trends for next action prediction, for the Breakfast dataset. The time line indicates the time distance to the next action, for each occurrence of the indicated action, in the video dataset.

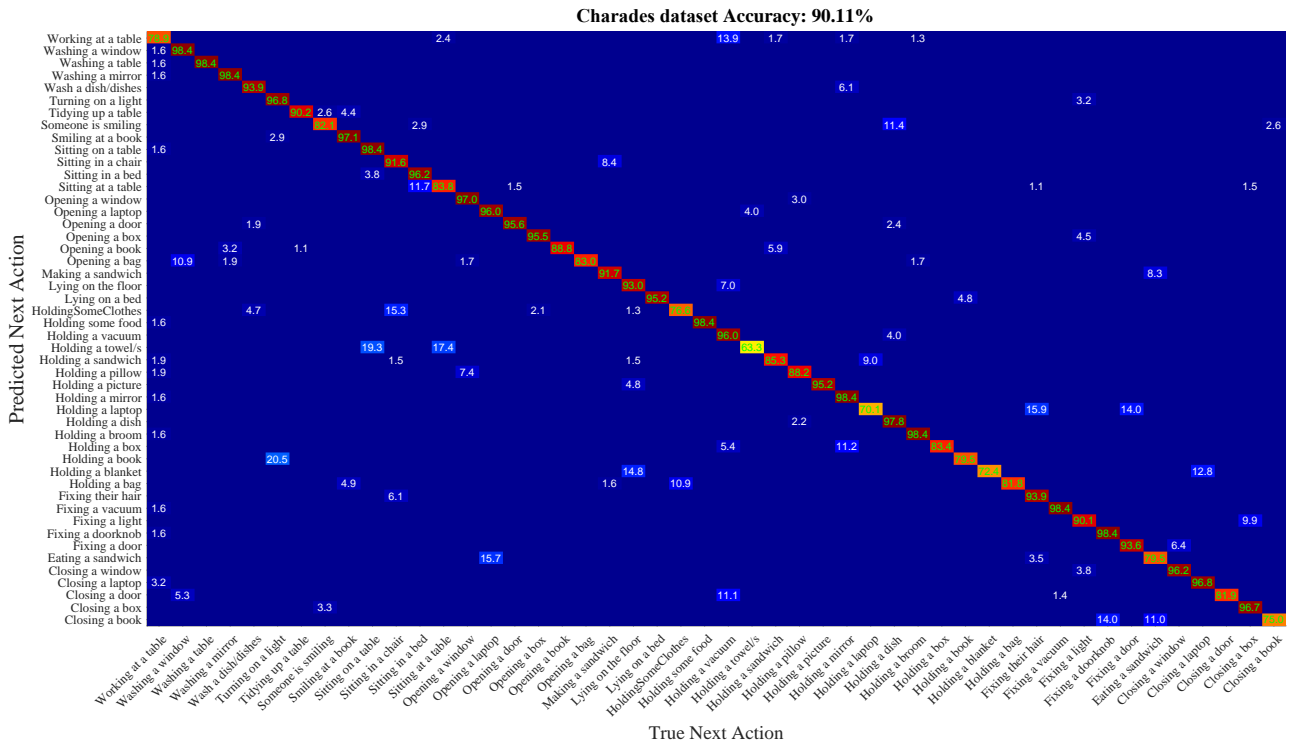


Figure 7: Confusion matrix for the CHARADES dataset. The heat-map is *jet*, values less than 1 are not shown.

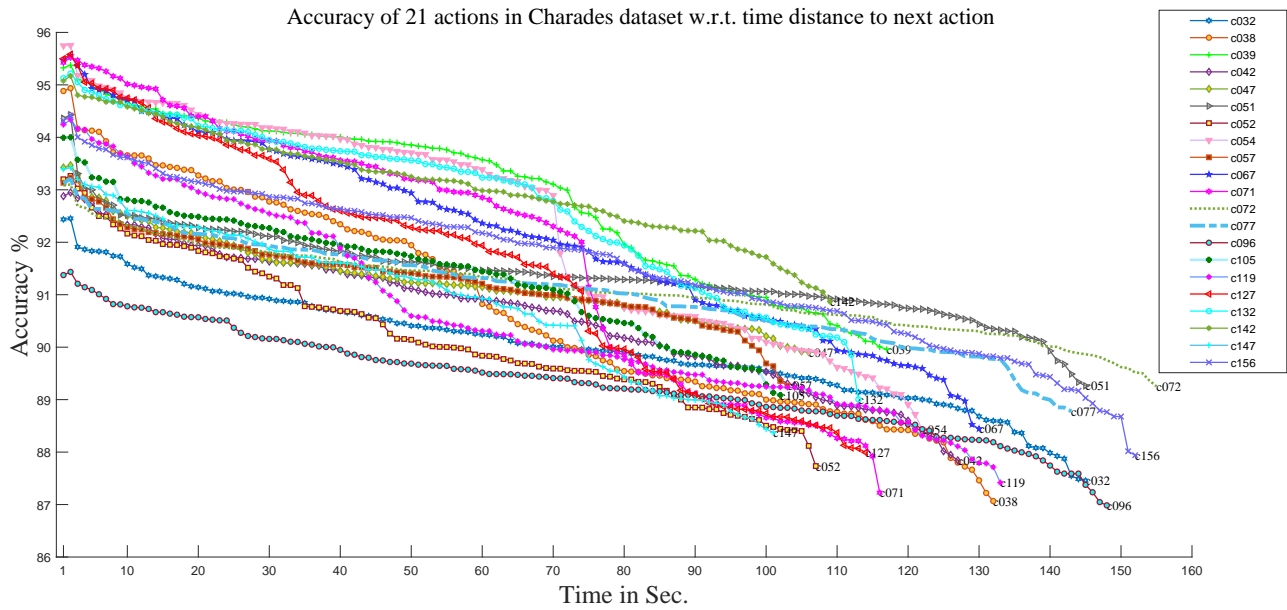


Figure 8: Accuracy trends for next action forecasting, in CHARADES dataset. The codes for actions are those used in CHARADES since action names are often very long. Here the codes are used to avoid clumsiness.